





Article

CO₂ Reduction to Valuable Chemicals on TiO₂-Carbon Photocatalysts Deposited on Silica Cloth

Antoni Waldemar Morawski ¹, Katarzyna Ćmielewska ^{1,*}, Kordian Witkowski ¹, Ewelina Kusiak-Nejman ¹, Iwona Pelech ¹, Piotr Staciwa ¹, Ewa Ekiert ¹, Daniel Sibera ^{1,2}, Agnieszka Wanag ¹, Marcin Gano ¹ and Urszula Narkiewicz ¹

¹ Department of Inorganic Chemical Technology and Environment Engineering, Faculty of Chemical Technology and Engineering, West Pomeranian University of Technology in Szczecin, Pulaskiego 10, 70-322 Szczecin, Poland; Antoni.Morawski@zut.edu.pl (A.W.M.); wk44867@zut.edu.pl (K.W.); Ewelina.Kusiak@zut.edu.pl (E.K.-N.); Iwona.Pelech@zut.edu.pl (I.P.); piotr.staciwa@zut.edu.pl (P.S.); Ewa.Dabrowa@zut.edu.pl (E.E.); Daniel.Sibera@zut.edu.pl (D.S.); Agnieszka.Wanag@zut.edu.pl (A.W.); Marcin.Gano@zut.edu.pl (M.G.); Urszula.Narkiewicz@zut.edu.pl (U.N.)

² Department of General Civil Engineering, Faculty of Civil and Environmental Engineering, West Pomeranian University of Technology in Szczecin, Piastow 50a, 70-311 Szczecin, Poland

* Correspondence: katarzyna.przywecka@zut.edu.pl

Abstract: A new photocatalyst for CO₂ reduction has been presented. The photocatalyst was prepared from a combination of a commercial P25 with a mesopore structure and carbon spheres with a microporous structure with high CO₂ adsorption capacity. Then, the obtained hybrid TiO₂-carbon sphere photocatalysts were deposited on a glass fiber fabric. The combined TiO₂-carbon spheres/silica cloth photocatalysts showed higher efficiency in the two-electron CO₂ reduction towards CO than in the eight-electron reaction to methane. The 0.5 g graphitic carbon spheres combined with 1 g of TiO₂ P25 resulted in almost 100% selectivity to CO. From a practical point of view, this is promising as it economically eliminates the need to separate CO from the gas mixture after the reaction, which also contains CH₄ and H₂.

Keywords: photocatalysis; CO₂ reduction; carbon-TiO₂



Citation: Morawski, A.W.; Ćmielewska, K.; Witkowski, K.; Kusiak-Nejman, E.; Pelech, I.; Staciwa, P.; Ekiert, E.; Sibera, D.; Wanag, A.; Gano, M.; et al. CO₂ Reduction to Valuable Chemicals on TiO₂-Carbon Photocatalysts Deposited on Silica Cloth. *Catalysts* **2022**, *12*, 31. <https://doi.org/10.3390/catal12010031>

Academic Editors: Javier Ereña Loizaga and Ainara Ateka

Received: 1 December 2021

Accepted: 22 December 2021

Published: 28 December 2021

Publisher's Note: MDPI stays neutral with regard to jurisdictional claims in published maps and institutional affiliations.



Copyright: © 2021 by the authors. Licensee MDPI, Basel, Switzerland. This article is an open access article distributed under the terms and conditions of the Creative Commons Attribution (CC BY) license (<https://creativecommons.org/licenses/by/4.0/>).

1. Introduction

Over the last 35 years, the annual CO₂ concentration in the atmosphere has increased from about 347 ppm to about 416 ppm [1]. At the same time, the average temperature increased by 0.7 °C. When the CO₂ concentration reaches 550 ppm, the estimated average temperature will increase by 2.0 °C [2]. Direct utilization of solar energy for photocatalytic reduction of carbon dioxide is still an important and elegant challenge for researchers to reduce atmospheric warming and climate change. Moreover, it can reduce the number of processes related to CO₂ disposal because it is carried out at atmospheric pressure and at room temperature. The photocatalytic conversion of CO₂ could lead to valuable products, such as hydrogen, carbon monoxide, methane, methanol, formaldehyde, formic acid, ethanol, and higher hydrocarbons. The nature of the products and the selectivity depend on the photocatalyst types and their modifications, the presence of water, and the chemical nature of their support [2–4].

Currently, many scientific publications consider the modification of TiO₂. Photocatalysis with UV-Vis radiation is one of the most intensively studied fields. According to the Scopus database, about 8400 publications in this field were published in 2021. Finding the additives that prevent the recombination of the electron-hole pair is highly desirable. They should also have the ability to shift the radiation absorption band towards the visible waves.

The modifiers are metals, metal oxides, and nonmetals, of which carbon in all its allotropes seems to be the most important [3,5]. When the reaction is considered in the

gas phase, it turns out that the nature of photocatalyst support significantly alters its properties. An example is the photoreduction of carbon dioxide over Fe-, Co-, Ni-, and Cu-incorporated TiO₂ on basalt fiber films. In this case, the CO₂ reduction to methane with high selectivity was caused by a synergistic effect. This effect was induced by the promotion of the photogenerated electron-hole pair (e[−]/h⁺) separations and also by the enhanced CO₂ adsorption [6].

For some time, carbon and its various allotropes have been considered as effective titanium dioxide modifiers that improve the adsorption capacity of the photocatalyst, as well as its photoactivity. It prevents the recombination of the electron-hole pair and shifts the adsorption band towards visible light. These properties relate to reactions in water and gas environments.

The pioneering series of works was initiated by J.-M. Herrmann [7–10]. The introduction of commercial activated carbon in contact with TiO₂ accelerates the synergistic effect and increases the reaction rate of phenol degradation by a factor of 2.5 [7]. Different activated carbons were tested to confirm this observation [8]. When 4-chlorophenol was selected as a model aromatic pollutant, the same result was obtained [9]. Different types of hazardous wastes were studied, including herbicides [10].

In the modification of carbon, we distinguish the following types of interactions of TiO₂ with carbon: carbon-doped TiO₂, carbon-coated TiO₂, and TiO₂-loaded carbon [11]. Enhanced adsorption and interaction of carbon with oxygen vacancies were postulated to be responsible for the higher activity.

One of the directions of modification of TiO₂ for photocatalytic reduction of CO₂ is the use of carbon nanotubes [12] or graphene [3,13]. Many scientists consider the electron transfer between TiO_{2−x} and graphene through Ti-O-C bonds [5]. The enhanced photoactivity was mainly attributed to the presence of graphene, which has an excellent ability to transport and collect electrons [13].

Peng Wang et al. [14] demonstrated a new carbon-doped amorphous titanium oxide for photocatalytic CO₂ reduction, prepared by sol-gel method. The best photocatalyst was prepared after annealing at 300 °C with yields of CH₄ and CO of 4.1 and 2.5 μmol/g/h for solar light, and 0.53 and 0.63 μmol/g/h for visible light, respectively.

J. Liu et al. [15] proposed a TiO₂-graphene nanocomposite prepared using GO and TiO₂ nanoparticles mixed in a suspension with water, sonicated, and then heated in an oil bath. The photoactivity upon reduction of CO₂ to CH₄ (2.1 μmol/g/h) and CH₃OH (2.2 μmol/g/h) was attributed to the synergistic effect between TiO₂ and graphene.

Tianyu Zhang et al. [16] have shown that the modification of graphene quantum dots by functional -OH and -NH₂ electron-donating groups increases the yield of CH₄ from CO₂ electroreduction with Faradaic efficiency by 70%.

The adsorption of CO₂ on the surface or the volume absorption on the photocatalyst is an important step in the photoreduction of CO₂. It is crucial especially in the gas-phase reaction. Therefore, in this work, we have investigated the preparation of composites of TiO₂ and carbon spheres using a simple method proposed by Herrmann [7–10], which consists of the mechanical mixing of TiO₂ with carbon material. The basis for this research direction was our previous work describing the high CO₂ adsorption capacity on the microporous carbon spheres of the graphitic structures we fabricated [17]. Proper management of adsorption and photoactivity by selecting a sorbent hybridized with TiO₂ leads to an increase in CO₂ reduction efficiency [18]. Finally, the above composite material was deposited on a glass fiber cloth which formed the photocatalytic bed in the reactor.

2. Results and Discussion

2.1. Characterization of Photocatalysts

The XRD patterns of the initial carbon spheres used for the nanocomposite production (Figure 1) showed two diffraction peaks of carbon at about 23° and 43°. The first peak corresponds to the stacking carbon layer structure (002) related to the parallel and azimuthal orientation of the aromatic and carbonized structures. The high symmetry of the peak

can suggest the absence of γ -bands linked to amorphous and aliphatic structures [19]. The second peak of lower intensity observed at 43° corresponds to the ordered graphitic and hexagonal carbon structures (100) [20]. The broadening of (100) peak indicates a low degree of aromatic ring condensation (low degree of graphitization) [21,22]. The (001) peak becomes more intense and sharper when carbon spheres are prepared at higher temperatures; then the degree of graphitization increases, and some graphene flakes can be observed in SEM images.

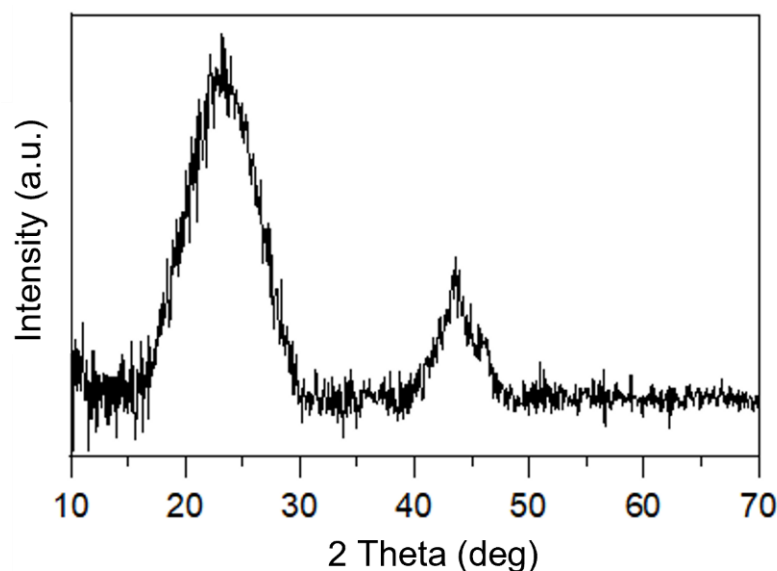


Figure 1. X-ray diffraction pattern of the starting carbon spheres.

In the case of carbon spheres used here, the temperature was lower and no graphene flakes can be observed in the SEM image shown in Figure 2. The produced spheres have a regular spherical shape and a smooth surface; neither defects nor inclusions can be observed. The size distribution is narrow, and the spheres are homogeneous and have an average diameter of about 600 nm.

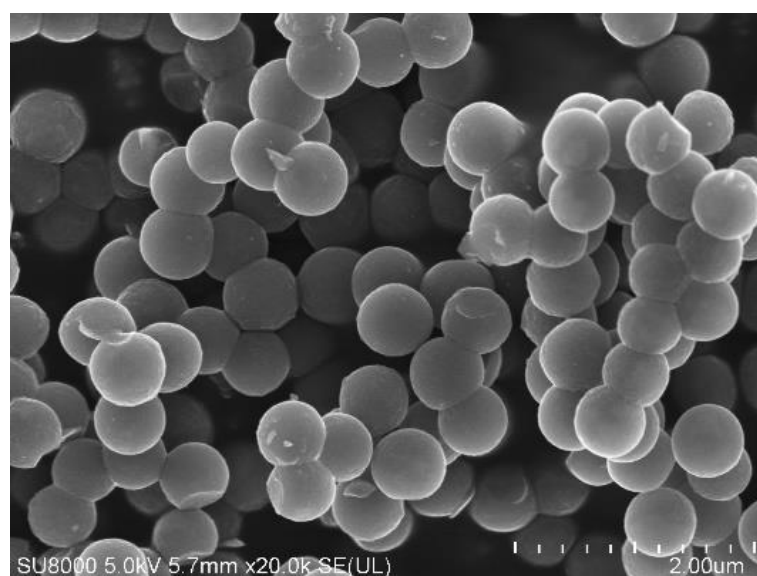


Figure 2. SEM image of the used carbon spheres.

The surface area of the spheres determined by the BET methods was 455 m²/g, dominated by ultrapores and micropores (Table 1). These characteristics affected CO₂ adsorption to 3.25 mmol/g and 2.43 mmol/g at temperatures of 0 °C and 25 °C, respectively.

Table 1. Textural parameters and CO₂ sorption capacities of pure carbon spheres.

Material	S _{BET} (m ² /g)	TPV (cm ³ /g)	V _s (<1 nm) (cm ³ /g)	V _m (<2 nm) (cm ³ /g)	V _{meso} (cm ³ /g)	CO ₂ 0 °C (mmol/g)	CO ₂ 25 °C (mmol/g)
CS	455	0.26	0.19	0.22	0.04	3.25	2.43

S_{BET}—specific surface area; TPV—total pore volume; V_s—the volume of ultramicropores with diameters smaller than 1 nm; V_m—the volume of micropores with diameters smaller than 2 nm; V_{meso}—the volume of mesopores with diameters from 2 to 50 nm.

The diffraction pattern of pure TiO₂ P25 is shown in Figure 3. The used titanium dioxide consisted of anatase (89%) and rutile (11%) with a crystallite size of 27 nm for anatase and 43 nm for rutile, as shown in Table 2. The energy gap calculated by the Kubelka–Munk theory was estimated as E_g = 3.204 eV. The determined BET surface area was 54 m²/g, dominated by the mesopore structure (Table 3). This is quite a difference compared to the carbon spheres. The adsorption of CO₂ was also much lower compared to the carbon spheres; 0.72 mmol/g for P25 at 30 °C [23] compared to 2.43 mmol/g at 25 °C for the carbon spheres.

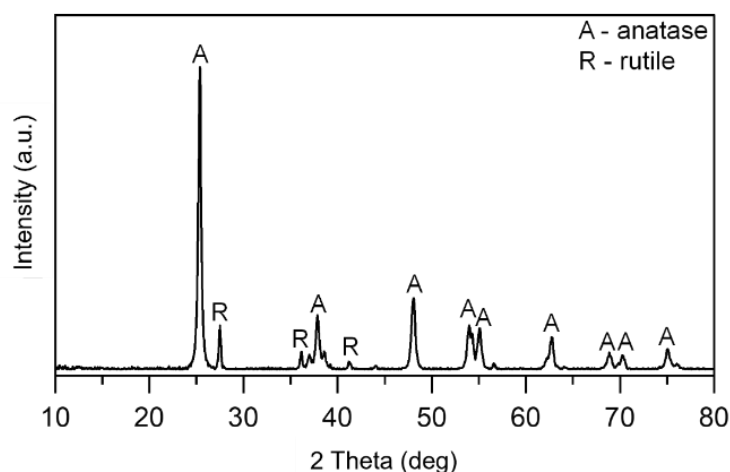


Figure 3. X-ray diffraction pattern of TiO₂ P25.

Table 2. Phase and crystallite composition of used P25.

Name	Phase Composition (%)		Crystallite Size (nm)	
	Anatase	Rutile	Anatase	Rutile
TiO ₂ P25	89	11	27	43

Table 3. Textural parameters of used P25.

Material	S _{BET} (m ² /g)	V _{total 0.95} (m ³ /g)	V _{mikro DR} (cm ³ /g)	V _{mezo} (cm ³ /g)	CO ₂ 30 °C (mmol/g)
TiO ₂ P25	54	0.4	0.02	0.38	0.72

From the photos taken with the scanning microscope, it can be observed that TiO_2 P25 nanocrystallites form relatively large, noncircular agglomerates with dimensions in the range of about 0.5–2 μm (Figure 4).

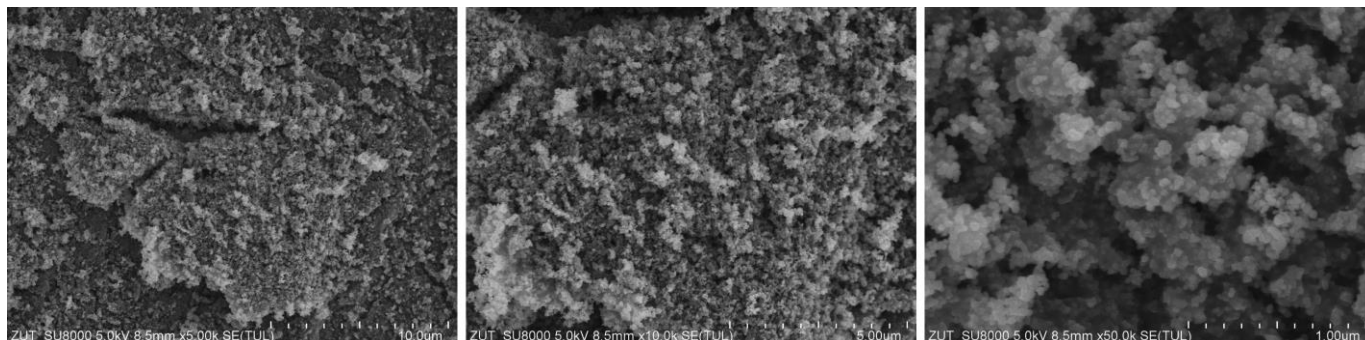


Figure 4. SEM images for used TiO_2 P25.

In the SEM images of pure silica fabric (Figure 5), one can see the fibers bound with a binder that provides a matrix for the applied photocatalysts. The surfaces of the fibers are virtually clear and smooth. EDX mapping shows that only Si, O, Al, and Ca originate from the fibers and the inorganic binder.

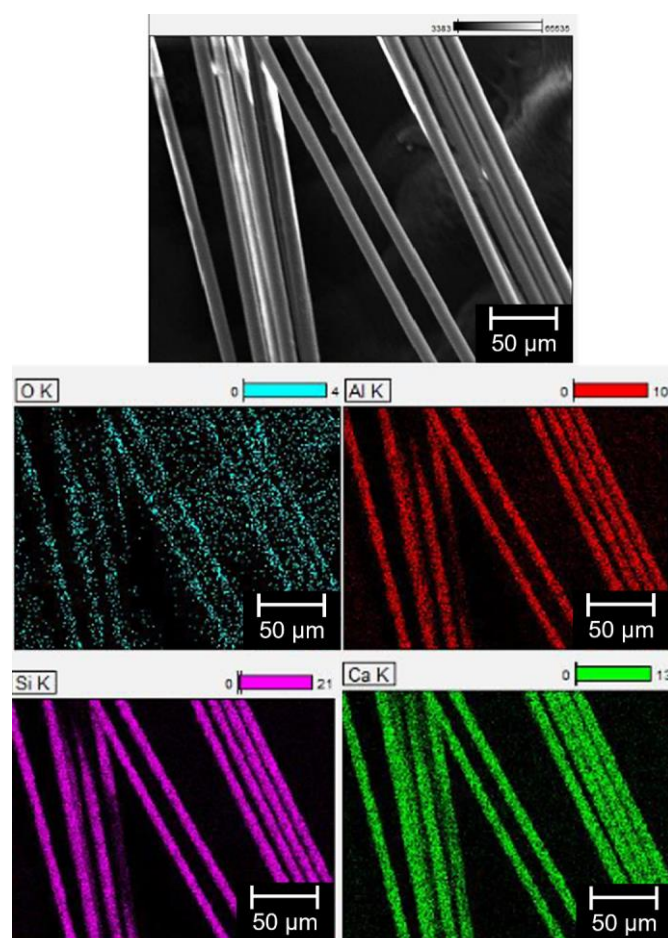


Figure 5. SEM images and EDX chemical element mappings of pure silica cloth.

Figure 6 presents photos of the prepared materials showing the dispersion of the photocatalysts on the silica fiber matrix. The dispersion of the TiO_2 P25 photocatalyst is

quite homogenous. The EDS analysis showed that the fibers are composed of silica and alumina with a Si/Al ratio of about 5/1. The matrix also contains calcium. The active phase, Ti in the form of TiO_2 , is present in a constant amount of about 10 wt% in each sample. The photocatalyst is dispersed on the surface of the fibers and the binder is located in particular between the layers of the fibers.

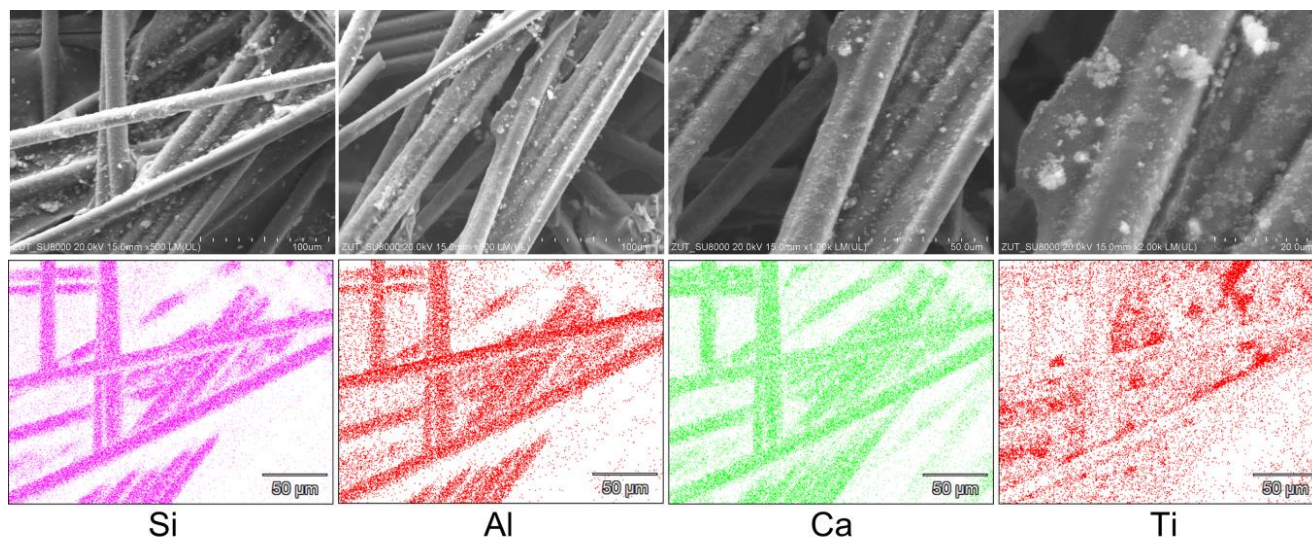


Figure 6. SEM images and EDX chemical element mappings of silica cloth coated by TiO_2 P25.

From the SEM photos presented in Figure 7, it can be seen that as the carbon spheres content is increased from 0.05 to 0.5, the number of agglomerates increases slightly. Of course, the shape of agglomerates characteristic of TiO_2 P25 dominates since the content of carbon spheres is lower in contrast to TiO_2 .

As in the case of the silica fabric coated with pure TiO_2 (Figure 6), almost the same properties are observed for the samples with different carbon content (Figure 7). Therefore, Figure 8 shows element mappings for the sample P25 + C 1/0.5 as an example. The analysis of EDS has shown that the fibers are composed of silica and alumina with a ratio of Si/Al of about 5/1 and also calcium, as can be seen in Table 4. The distributions of Si, O, and Ca indicate that these elements are constituents of the fiber. The active phase of Ti in the form of TiO_2 is present in each sample in a constant amount of about 10 wt%. It is located on the surface of the fibers, mainly in the form of agglomerates.

2.2. Photocatalytic Activity Measurements

Figure 9a–d present the ability to photoreduce carbon dioxide with water vapor to carbon monoxide (CO), methane (CH_4), and hydrogen (H_2), respectively, with reaction times given in $\mu\text{mol}/\text{g}_{\text{photocatalyst}}/\text{dm}^3$.

The addition of carbon spheres in an amount of 0.05 g per 1 g of TiO_2 resulted in a slight increase in the photocatalyst activity (Figure 9b) compared to pure P25 (Figure 9a). The comparison of the photoactivity towards CO production is presented in Figure 10. The amount of carbon monoxide produced decreased slightly from $55.75 \mu\text{mol}/\text{g}_{\text{photocatalyst}}/\text{dm}^3$ for P25 and $55.94 \mu\text{mol}/\text{g}_{\text{photocatalyst}}/\text{dm}^3$ for P25 + C 1/0.05 to $43.62 \mu\text{mol}/\text{g}_{\text{photocatalyst}}/\text{dm}^3$ for the sample P25 + C 1/0.1 and to $46.79 \mu\text{mol}/\text{g}_{\text{photocatalyst}}/\text{dm}^3$ in the case of the P25 + C 1/0.5 material. At the same time, the amount of methane decreased significantly and gradually from $9.02 \mu\text{mol}/\text{g}_{\text{photocatalyst}}/\text{dm}^3$ (pure P25) through 4.76 and $4.02 \mu\text{mol}/\text{g}_{\text{photocatalyst}}/\text{dm}^3$ for materials P25 + C 1/0.05 and P25 + C 1/0.1, respectively; to practically $0.00 \mu\text{mol}/\text{g}_{\text{photocatalyst}}/\text{dm}^3$ in the case of the P25 + C 1/0.5 sample.

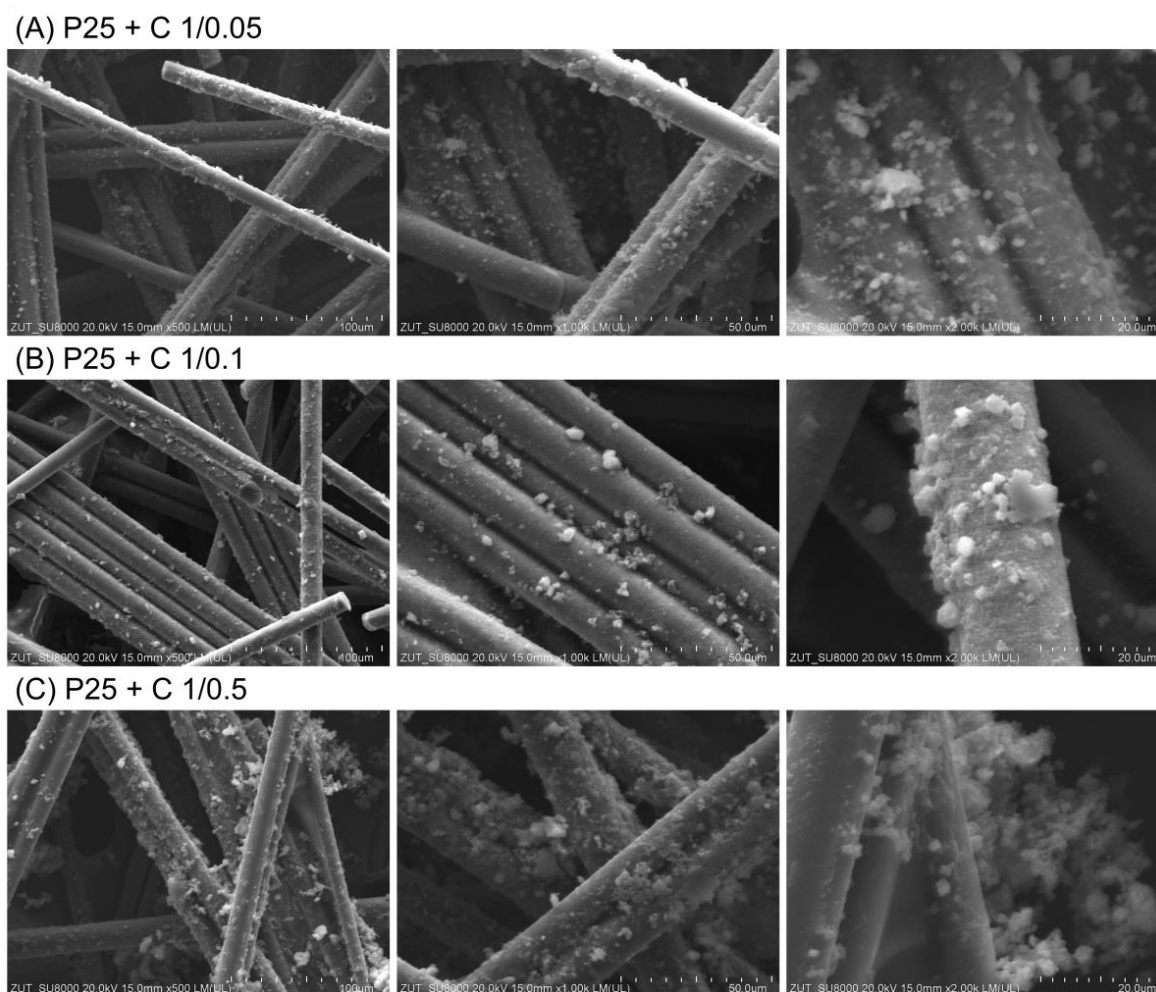


Figure 7. SEM images of silica cloth coated by TiO_2 P25 combined with different amount of carbon spheres; (A) P25 + C 1/0.05; (B) P25 + C 1/0.1; (C) P25 + C 1/0.5.

From the results obtained, it can be seen that the amount of methane captured decreased with the increasing carbon content in the material (Figure 11). The same dependence was also observed for the hydrogen production (Figure 12).

Two factors may contribute to the decrease in the photoactivity for CO , CH_4 , and H_2 with the increasing carbon sphere content. The first aspect is the well-known electron interaction between amphoteric electrons from the surface of the graphite spheres and the functional groups of the TiO_2 surface. This prevents the recombination of the electron-hole pair. It is known that even a small interaction, specifically doping [14], is necessary to achieve a positive effect. The addition of large amounts of carbon from 0.1 g/1 g TiO_2 to 0.5 g/1 g TiO_2 causes the scattering of electrons in the structure with a large amount of carbon.

The second effect is caused by the increased CO_2 adsorption by the carbon spheres, as shown in Table 1. TiO_2 adsorbs only 0.72 mmol CO_2 /g at 30 °C (Table 3), while carbon spheres adsorb 2.43 mmol CO_2 /g. A large addition of carbon spheres increases the sorption and the presence of CO_2 on the surface of the photocatalyst, which forms CO_3^{2-} ions in the presence of H_2O vapors, which are strong electron scavengers. The further addition of carbon spheres did not positively affect the activity. In the case of sample P25 + C 1/0.5 (Figure 9d), the only product of the process was carbon monoxide. The higher content of carbon spheres blocked the UV-Vis radiation, which can generate the TiO_2 electron-hole pair and, at the same time, scatter and disperse the excited electrons in the crystal lattice of the carbon spheres.

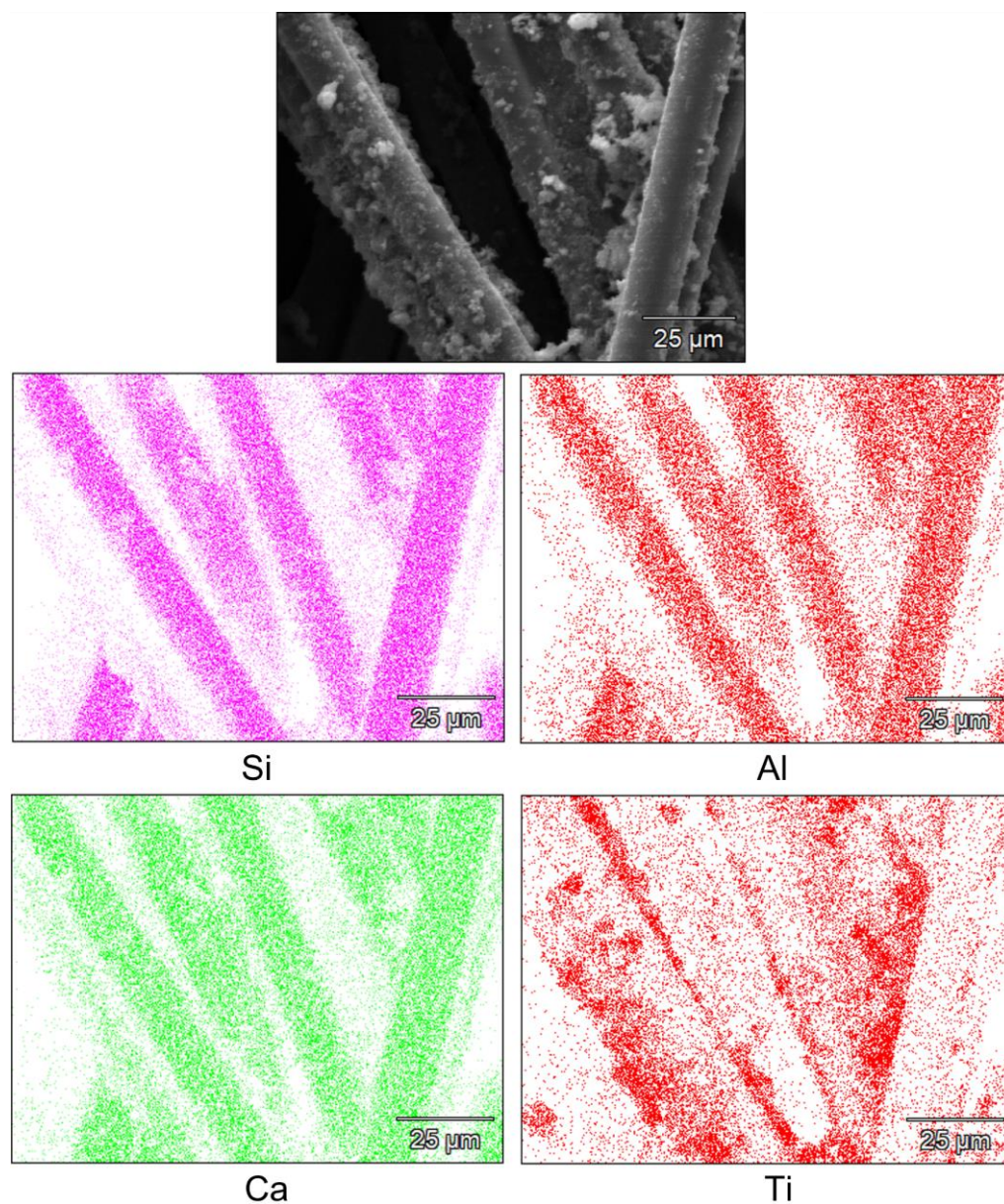


Figure 8. Example of EDX chemical element mappings of silica cloth coated by TiO_2 P25 combined with carbon spheres for sample P25 + C 1/0.5.

Table 4. Surface chemical element compositions from EDX of silica cloth coated by TiO_2 P25 combined with carbon spheres for sample P25 + C 1/0.5.

Chemical Element	Weight (wt%)	Atom (%)
C	18.69	37.17
O	9.33	13.93
Al	4.96	4.39
Si	25.42	21.62
Ca	21.77	12.97
Ti	19.55	9.75
K	0.28	0.17

It can be observed that the main products are CO, CH₄, and H₂. Carbon monoxide is also the dominant component of the postreaction gases, regardless of the amount of carbon spheres added as a modifier.

The reactivity of the photocatalysts is probably limited by the reduction of water to hydrogen, which is the first stage of the whole complex process. In our case, with the exception of sample P25 + C 1/0.5, there is some excess of hydrogen, which is a positive phenomenon.

Hydrogen is formed in the reactions at the photocatalysts, as reported by Peng Wang et al. [14] and Minoo Tasbihi et al. [24]:

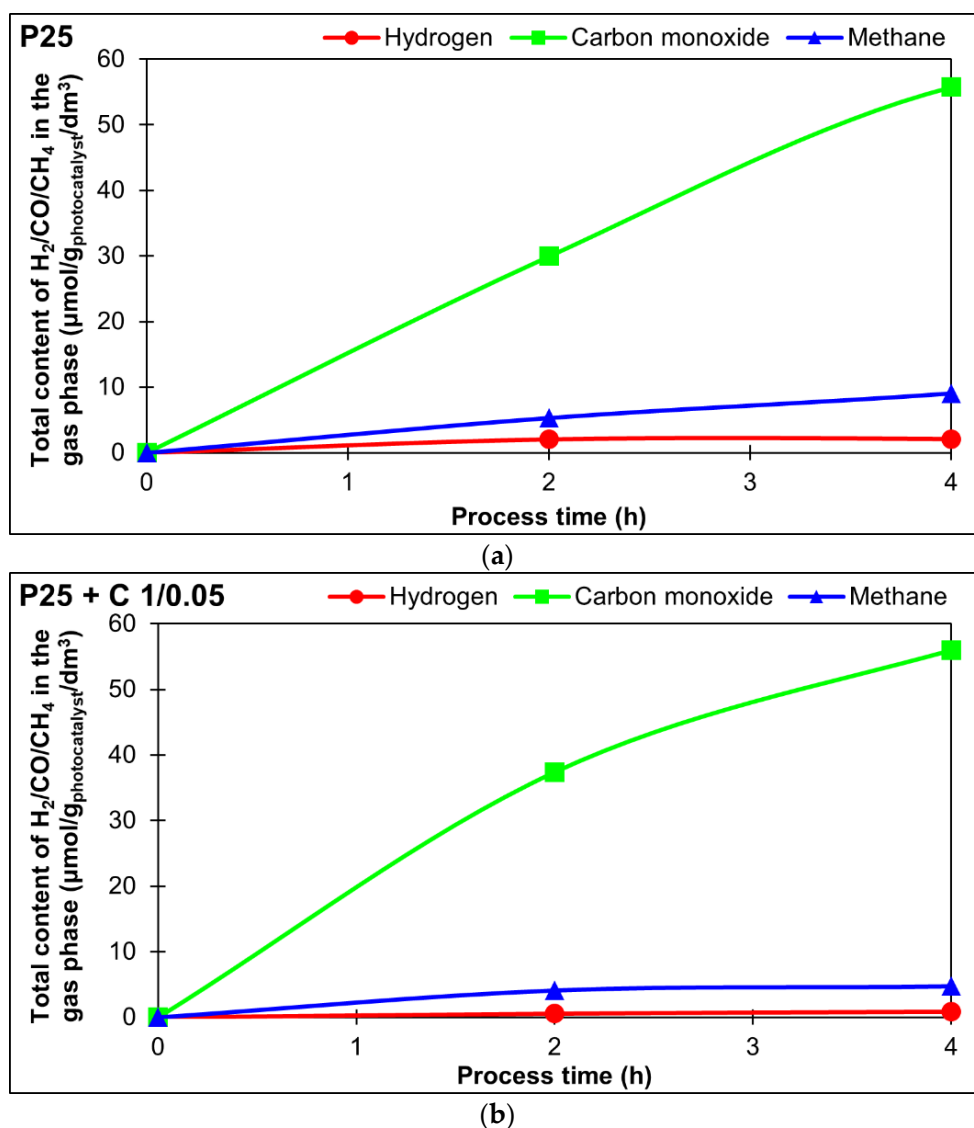


Figure 9. Cont.

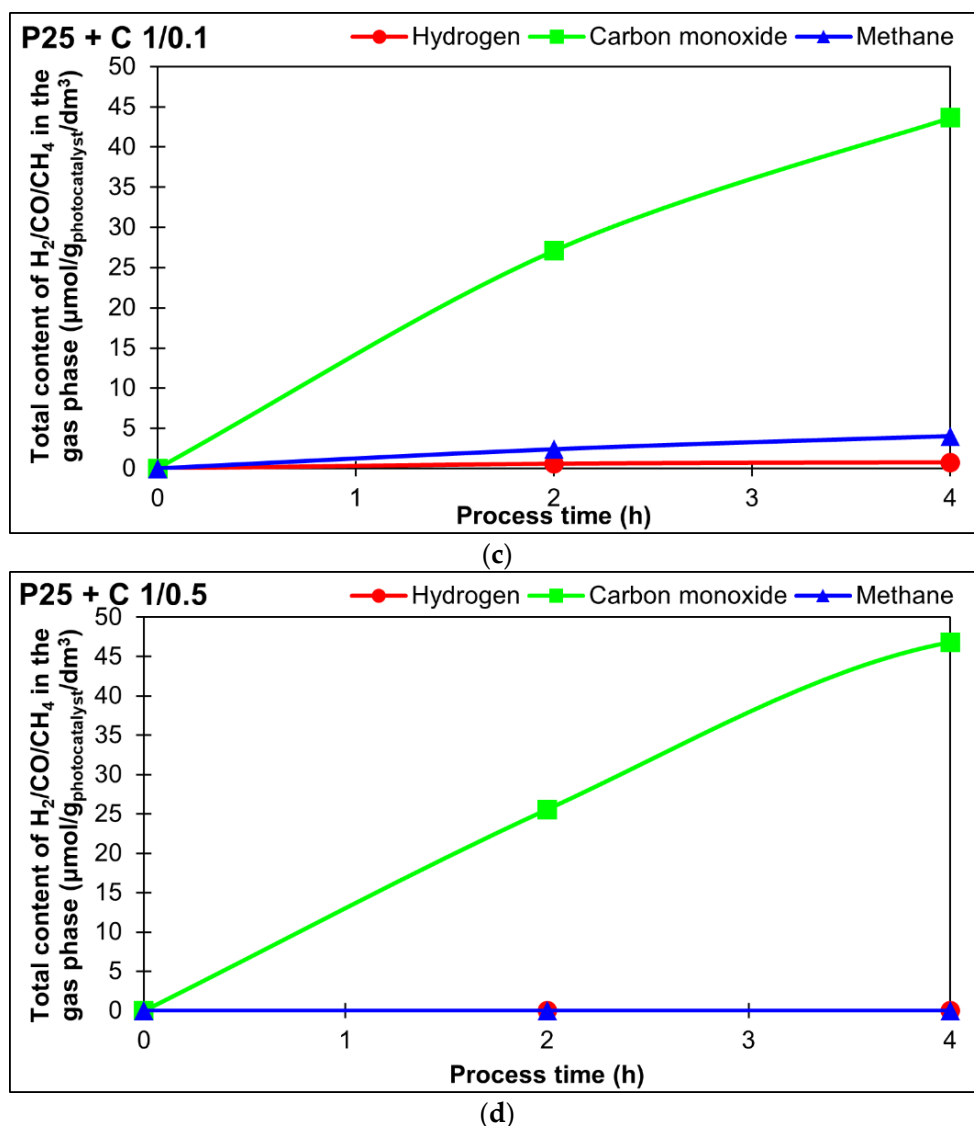
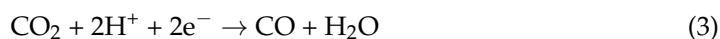
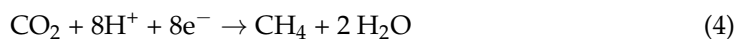


Figure 9. Total content of the products of the photoreduction of CO₂ in the process with: (a) P25, (b) P25 + C 1/0.05, (c) P25 + C 1/0.1, (d) P25 + C 1/0.5.

Carbon monoxide is the result of an easier two-electron reduction of carbon dioxide:



The lower efficiency of the reaction towards methane production is the result of the more difficult eight-electron CO₂ reduction reaction:



On the homogeneous surface of the photocatalyst, reactions No. 1 to No. 4 are the two-electron production of hydrogen (reactions 1–2) and a two-electron to carbon monoxide (reaction No. 3), which could be considered as an intermediate step to the 8-electron reaction of No. 4 towards methane.

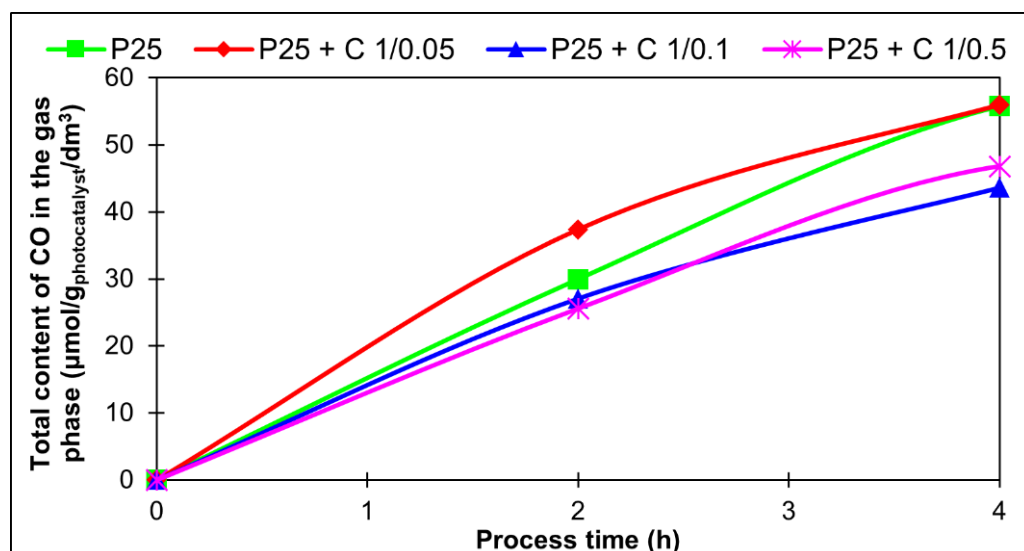


Figure 10. Total content of carbon monoxide of the photoreduction of CO_2 for the studied samples: P25; P25 + C 1/0.05; P25 + C 1/0.1, and P25 + C 1/0.5.

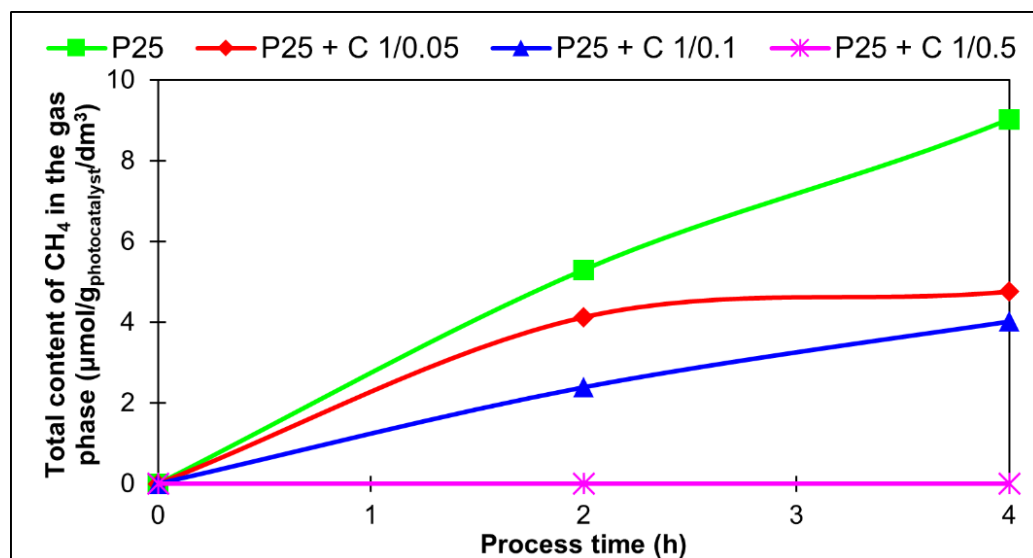


Figure 11. Total content of methane in the photoreduction of CO_2 for the following photocatalysts: P25; P25 + C 1/0.05; P25 + C 1/0.1, and P25 + C 1/0.5.

It is known that the hydrogen production reactions (reactions No. 1–2 water splitting) take place in the semiconductor valence band (on holes), and the CO_2 reduction reactions take place in the conduction band (with the participation of electrons).

For this reason, the production of hydrogen controls all CO_2 reduction reactions. In this case, only the CO formation reaction (No. 3) and the methane forming reaction (No. 4) are linearly competing with each other. Indeed, as shown in Figure 13, with the addition of carbon spheres, excess hydrogen decreases, and at the same time, methane decreases, which requires more hydrogen than the formation of carbon monoxide in reaction No. 3.

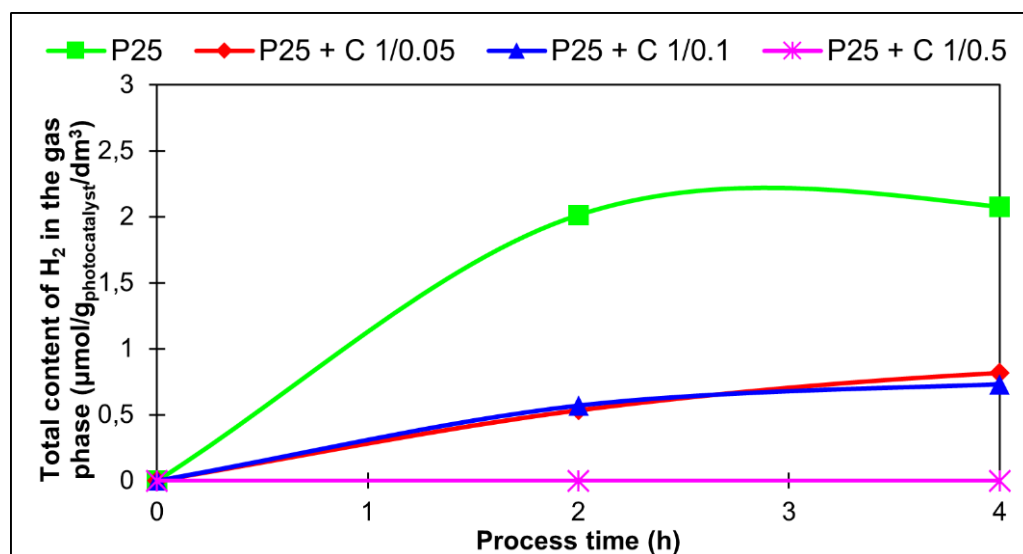


Figure 12. Total content of hydrogen in the photoreduction of CO₂ for subsequent photocatalysts: P25, P25 + C 1/0.05, P25 + C 1/0.1, and P25 + C 1/0.5.

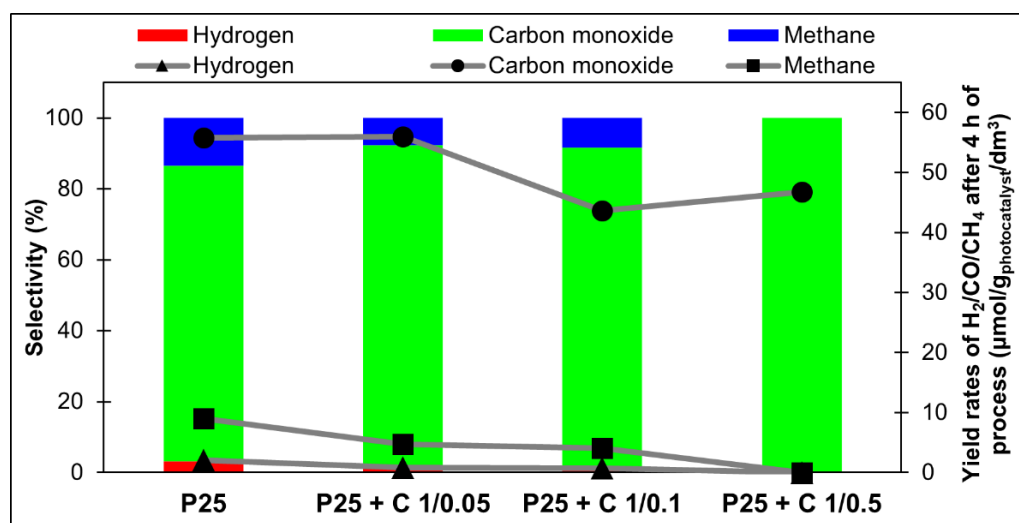


Figure 13. Selectivity and yield rates of the products after 4 h of the process.

The collected postreaction gas composition is different from that obtained on photocatalysts on mineralogical ground fibers, where only methane was obtained and no other components were identified [6]. In our case, by using silicon fibers, it is possible to obtain a mixture of CO, CH₄, and small amounts of hydrogen, with high selectivity to CO. Figure 13 shows the calculated selectivity, and the obtained amounts of each component of the gas phase produced. In all the cases tested, high selectivity to carbon monoxide is observed—from about 83.40% to 100% for the sample P25 + C 1/0.5, where the hydrogen was entirely consumed by the two-electron reaction of reduction of CO₂ to CO.

3. Experimental

3.1. Preparation of the Samples

In the experiments, photocatalysts consisting of TiO₂ P25, manufactured by Degussa (Evonik Industries AG, Germany), and carbon material were tested. The carbon material was prepared with the use of resorcinol and formaldehyde. The description of the original method of producing carbon spheres used in this work is presented elsewhere [25]. Three

powders with different mass ratios of titanium dioxide to carbon were prepared by grinding in a mortar. The mass ratios were: 1:0.05; 1:0.1, and 1:0.5. Aqueous suspensions of the prepared materials were applied to the fiberglass cloth. Glass fiber fabric with an area weight of 40 g/m² was supplied by Fiberglass Fabrics (Opole, Poland). Then the fibers with the photocatalysts were dried at 110 °C for 1 h.

3.2. Photoreduction Process

Experiments were performed in a cylindrical quartz reactor with a working volume of 392 cm³ (Figure 14). Four Actinic BL TL-E Philips lamps were used with a total power of 88 W, emitting UV-A radiation in the wavelength range of 350–400 nm. The lamps were located outside the reactor and formed a ring. The reactor was sealed in a thermostatic chamber to exclude other light sources and ensure a stable process temperature. An amount of 1 cm³ of distilled water was poured into the reactor. A photocatalyst previously applied to glass fibers was added to the reactor. Then the whole system was purged with pure CO₂ (Messer, Poland) for 30 min. After this time, the system was tightly sealed and the lamps were turned on. Both during purging and during the process, the gas was stirred using a pump with a flow rate of 1.6 dm³/h. The process was carried out for 4 h. Gas samples were collected every 2 h for analysis.

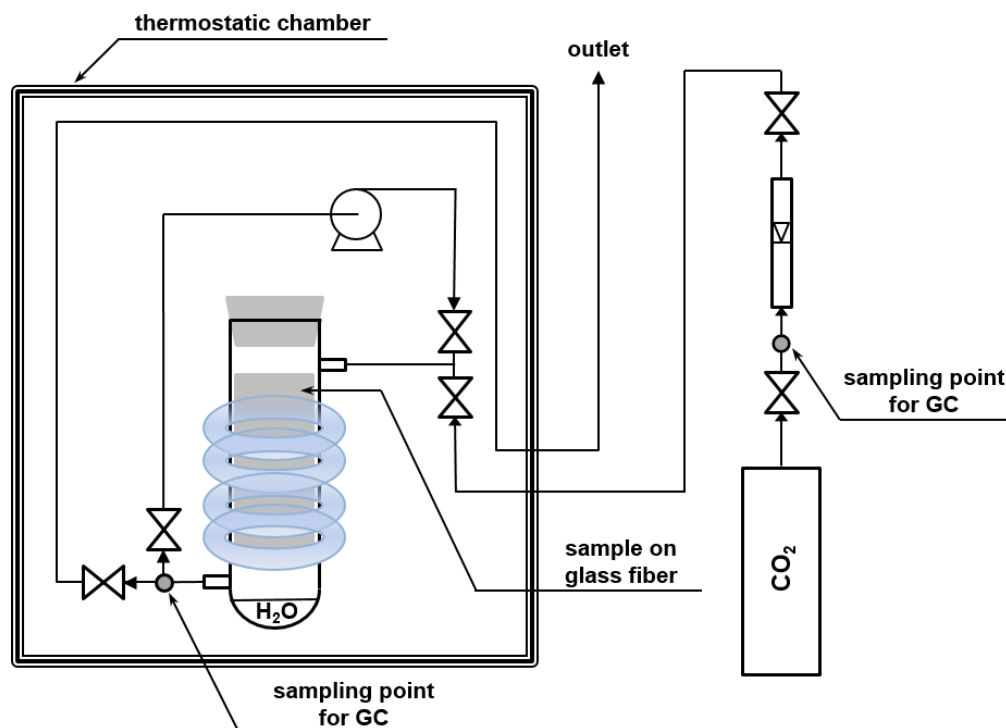


Figure 14. The scheme of the reactor for photocatalytic reduction of CO₂ in the gas phase.

3.3. The Analysis of the Gas Phase

The gas phase composition was analyzed using SRI 310C gas chromatograph (SRI Instruments, Torrance, CA, USA), equipped with a 5 Å molecular sieve column and an HID detector (Helium Ionization Detector). The carrier gas was helium. The analyses were performed under isothermal conditions at 60 °C. The gas flow through the column was 60 cm³/min, while the volume of the gas sample was 1 cm³. The content of each component in the gas phase was calculated in the subsequent measurements based on the calibration curve.

3.4. XRD Analysis

The crystalline structure of used titanium dioxide and carbon spheres was studied with X-ray powder diffraction (CuK α radiation, Malvern PANalytical B.V., The Netherlands). The mean crystallites sizes were calculated based on Scherrer's equation:

$$D = \frac{K\lambda}{\beta \cos \theta} \quad (5)$$

where:

D —mean crystallite size (nm),

λ —wavelength of Cu K α radiation (nm),

θ —Bragg's angle ($^{\circ}$),

β —calibrated width of a diffraction peak at half maximum intensity (rad).

The percentage of anatase in the crystalline phase (%A) was calculated according to the equation:

$$\%A = \frac{I_A}{I_A + I_R} \cdot 100\% \quad (6)$$

where I_A and I_R are the diffraction intensities of the anatase peak at 25.4° and rutile peak at 27.5° , respectively.

3.5. SEM/EDS Measurements

The surface morphology of the samples was examined using a scanning electron microscope (SEM Hitachi SU 8020, Japan). The SEM and EDS analysis parameters were: acceleration voltage of 20 kV and current of 10 μ A. The samples for investigation using SEM were firstly vapor-deposited with a 5 nm thin chromium layer to protect the samples from the electrical charge.

3.6. Textural Parameters and CO₂ Sorption Capacity Analysis

The specific surface areas (S_{BET}) were calculated from the Brunauer–Emmett–Teller equation, based on the nitrogen adsorption isotherms measured at 77 K using QUADRA-SORB evoTM Gas Sorption analyzer (Anton Paar GmbH, Austria) in the relative pressure range of 0.05–0.2. Before the measurements, the materials were degassed for 12 h at 105 $^{\circ}$ C under the high vacuum. The total pore volume (V_{total}) was determined on the basis of the maximum adsorption of nitrogen vapor at $p/p_0 = 0.95$. Micropore volume (V_{micro}) was calculated using the Dubinin–Radushkevich method, while the mesopore volume (V_{meso}) was obtained from the difference between V_{total} and V_{micro} .

Adsorption of the carbon dioxide was performed at 0 $^{\circ}$ C and 25 $^{\circ}$ C using the same QuadrasorbTM automatic system (Quantachrome Instruments) in the pressure range between 0.01 and 0.98 bar.

Adsorption of the carbon dioxide was also measured at 30 $^{\circ}$ C with the use of the TGA method (Netzsch STA 449 C, Netzsch GmbH, Germany). The flow rate of carbon dioxide during the analysis was 30 cm³/min. The process of adsorption of CO₂ by the tested material lasted 120 min.

4. Conclusions

A relatively simple method for the preparation of a photocatalyst was presented in which TiO₂ was combined with carbon spheres, which were then deposited on a silica fiber cloth to provide a good bed for the photocatalytic reduction of CO₂ in the gas phase. The obtained TiO₂-carbon spheres/silica fiber photocatalysts showed high selectivity towards carbon monoxide. This is very promising from a practical point of view since the step of separating the carbon monoxide from the postreaction mixture can be avoided with only a slight reduction in the activity. For TiO₂ combined with a higher amount of graphitic carbon spheres, the two-electron reduction of CO₂ to CO is more privileged than an eight-electron reaction to methane.

Author Contributions: Conceptualization, A.W.M. and U.N.; methodology, A.W.M., E.K.-N., A.W. and K.Č.; software, M.G.; validation, A.W.M., U.N., E.K.-N. and I.P.; formal analysis, K.Č., K.W., E.E. and M.G.; investigation, A.W.M., K.Č. and K.W.; resources, U.N.; data curation, A.W.M. and U.N.; writing—original draft preparation, A.W.M. and K.Č.; writing—review and editing, K.Č., A.W.M., U.N., P.S. and D.S.; visualization, K.Č.; supervision, A.W.M. and U.N.; project administration, U.N.; funding acquisition, U.N. All authors have read and agreed to the published version of the manuscript.

Funding: The research leading to these results received funding from the Norway Grants 2014–2021 via the National Centre for Research and Development under the grant number NOR/POLNORCCS/PhotoRed/0007/2019-00.

Data Availability Statement: Not applicable.

Conflicts of Interest: The authors declare no conflict of interest.

References

1. Daily CO₂. Available online: <https://www.co2.earth/daily-co2> (accessed on 14 December 2021).
2. Al Jitan, S.; Palmisano, G.; Garlisi, C. Synthesis and Surface Modification of TiO₂-Based Photocatalysts for the Conversion of CO₂. *Catalysts* **2020**, *10*, 227. [CrossRef]
3. Fu, Z.; Yang, Q.; Liu, Z.; Chen, F.; Yao, F.; Xie, T.; Zhong, Y.; Wang, D.; Li, J.; Li, X.; et al. Photocatalytic Conversion of Carbon Dioxide: From Products to Design the Catalysts. *J. CO₂ Util.* **2019**, *34*, 63–73. [CrossRef]
4. Fu, J.; Jiang, K.; Qiu, X.; Yu, J.; Liu, M. Product Selectivity of Photocatalytic CO₂ Reduction Reactions. *Mater. Today* **2020**, *32*, 222–243. [CrossRef]
5. Zhang, J.; Tian, B.; Wang, L.; Xing, M.; Lei, J. *Photocatalysis. Fundamentals, Materials and Application*; Springer: Singapore, 2018.
6. Do, J.Y.; Kwak, B.S.; Park, S.M.; Kang, M. Effective Carbon Dioxide Photoreduction over Metals (Fe-, Co-, Ni-, and Cu-) Incorporated TiO₂/Basalt Fiber Films. *Int. J. Photoenergy* **2016**, *2016*, 5195138. [CrossRef]
7. Matos, J.; Laine, J.; Herrmann, J.-M. Synergy Effect in the Photocatalytic Degradation of Phenol on a Suspended Mixture of Titania and Activated Carbon. *Appl. Catal. B Environ.* **1998**, *18*, 281–291. [CrossRef]
8. Matos, J.; Laine, J.; Herrmann, J.-M. Association of Activated Carbons of Different Origins with Titania in the Photocatalytic Purification of Water. *Carbon N. Y.* **1999**, *37*, 1870–1872. [CrossRef]
9. Herrmann, J.-M.; Matos, J.; Disdier, J.; Guillard, C.; Laine, J.; Malato, S.; Blanco, J. Solar Photocatalytic Degradation of 4-Chlorophenol Using the Synergistic Effect between Titania and Activated Carbon in Aqueous Suspension. *Catal. Today* **1999**, *54*, 255–265. [CrossRef]
10. Matos, J.; Laine, J.; Herrmann, J.-M. Effect of the Type of Activated Carbons on the Photocatalytic Degradation of Aqueous Organic Pollutants by UV-Irradiated Titania. *J. Catal.* **2001**, *200*, 10–20. [CrossRef]
11. Morawski, A.; Janus, M.; Tryba, B.; Toyoda, M.; Tsumura, T.; Inagaki, M. Carbon Modified TiO₂ Photocatalysts for Water Purification. *Pol. J. Chem. Technol.* **2009**, *11*, 46–50. [CrossRef]
12. Rodríguez, V.; Camarillo, R.; Martínez, F.; Jiménez, C.; Rincón, J. CO₂ Photocatalytic Reduction with CNT/TiO₂ Based Nanocomposites Prepared by High-Pressure Technology. *J. Supercrit. Fluids* **2020**, *163*, 104876. [CrossRef]
13. Morawski, A.W.; Kusiak-Nejman, E.; Wanag, A.; Narkiewicz, U.; Edelmannová, M.; Reli, M.; Kočí, K. Influence of the Calcination of TiO₂-Reduced Graphite Hybrid for the Photocatalytic Reduction of Carbon Dioxide. *Catal. Today* **2021**, *380*, 32–40. [CrossRef]
14. Wang, P.; Yin, G.; Bi, Q.; Huang, X.; Du, X.; Zhao, W.; Huang, F. Efficient Photocatalytic Reduction of CO₂ Using Carbon-Doped Amorphous Titanium Oxide. *ChemCatChem* **2018**, *10*, 3854–3861. [CrossRef]
15. Liu, J.; Niu, Y.; He, X.; Qi, J.; Li, X. Photocatalytic Reduction of CO₂ Using TiO₂-Graphene Nanocomposites. *J. Nanomater.* **2016**, *2016*, 6012896. [CrossRef]
16. Zhang, T.; Li, W.; Huang, K.; Guo, H.; Li, Z.; Fang, Y.; Yadav, R.M.; Shanov, V.; Ajayan, P.M.; Wang, L.; et al. Regulation of Functional Groups on Graphene Quantum Dots Directs Selective CO₂ to CH₄ Conversion. *Nat. Commun.* **2021**, *12*, 5265. [CrossRef] [PubMed]
17. Morawski, A.W.; Staciwa, P.; Sibera, D.; Moszyński, D.; Zgrzebnicki, M.; Narkiewicz, U. Nanocomposite Titania–Carbon Spheres as CO₂ and CH₄ Sorbents. *ACS Omega* **2020**, *5*, 1966–1973. [CrossRef]
18. Liu, L.; Zhao, C.; Xu, J.; Li, Y. Integrated CO₂ Capture and Photocatalytic Conversion by a Hybrid Adsorbent/Photocatalyst Material. *Appl. Catal. B Environ.* **2015**, *179*, 489–499. [CrossRef]
19. Lu, L.; Kong, C.; Sahajwalla, V.; Harris, D. Char structural ordering during pyrolysis and combustion and its influence on char reactivity. *Fuel* **2002**, *81*, 1215–1225. [CrossRef]
20. Liu, X.; Song, P.; Hou, J.; Wang, B.; Xu, F.; Zhang, X. Revealing the Dynamic Formation Process and Mechanism of Hollow Carbon Spheres: From Bowl to Sphere. *ACS Sustain. Chem. Eng.* **2018**, *6*, 2797–2805. [CrossRef]
21. Kukułka, W.; Wenelska, K.; Baca, M.; Chen, X.; Mijowska, E. From Hollow to Solid Carbon Spheres: Time-Dependent Facile Synthesis. *Nanomaterials* **2018**, *8*, 861. [CrossRef]

22. Juhl, A.C.; Schneider, A.; Ufer, B.; Brezesinski, T.; Janek, J.; Fröba, M. Mesoporous hollow carbon spheres for lithium-sulfur batteries: Distribution of sulfur and electrochemical performance. *Beilstein J. Nanotechnol.* **2016**, *7*, 1229–1240. [[CrossRef](#)]
23. Kapica-Kozar, J.; Piróg, E.; Wrobel, R.J.; Mozia, S.; Kusiak-Nejman, E.; Morawski, A.W.; Narkiewicz, U.; Michalkiewicz, B. TiO₂/Titanate Composite Nanorod Obtained from Various Alkali Solutions as CO₂ Sorbents from Exhaust Gases. *Microporous Mesoporous Mater.* **2016**, *231*, 117–127. [[CrossRef](#)]
24. Tasbihi, M.; Kočí, K.; Troppová, I.; Edelmannová, M.; Reli, M.; Čapek, L.; Schomäcker, R. Photocatalytic Reduction of Carbon Dioxide over Cu/TiO₂ Photocatalysts. *Environ. Sci. Pollut. Res.* **2018**, *25*, 34903–34911. [[CrossRef](#)] [[PubMed](#)]
25. Pelech, I.; Sibera, D.; Staciwa, P.; Kusiak-Nejman, E.; Kapica-Kozar, J.; Wanag, A.; Narkiewicz, U.; Morawski, A.W.; Pl, A.W.M. ZnO/Carbon Spheres with Excellent Regenerability for Post-Combustion CO₂ Capture. *Materials* **2021**, *14*, 6478. [[CrossRef](#)] [[PubMed](#)]